

Linear and nonlinear optical probe of the ferroelectric-like phase transition in a polar metal, LiOsO₃

Haricharan Padmanabhan,¹ Yoonsang Park,¹ Danilo Puggioni,² Yakun Yuan,¹ Yanwei Cao,³ Lev Gasparov,⁴ Youguo Shi,⁵ Jak Chakhalian,³ James M. Rondinelli,² and Venkatraman Gopalan^{1, a)}

¹⁾ *Department of Materials Science and Engineering, The Pennsylvania State University, University Park, PA 16801, USA*

²⁾ *Department of Materials Science and Engineering, Northwestern University, Evanston, IL 60208, USA*

³⁾ *Department of Physics and Astronomy, Rutgers University, Piscataway, NJ 08854, USA*

⁴⁾ *Department of Physics, University of North Florida, 1 UNF Drive Jacksonville, FL 32224, USA*

⁵⁾ *Institute of Physics, Chinese Academy of Sciences, Beijing 100190, China*

(Dated: 18 September 2018)

LiOsO₃ is one of the first materials identified in recent literature as a 'polar metal', a class of materials that are simultaneously noncentrosymmetric and metallic. In this work, the linear and nonlinear optical susceptibility of LiOsO₃ is studied by means of ellipsometry and optical second harmonic generation (SHG). Strong optical birefringence is observed using spectroscopic ellipsometry. The nonlinear optical susceptibility extracted from SHG polarimetry reveals that the tensor components are of the same magnitude as in isostructural insulator LiNbO₃, except the component along the polar axis d_{33} , which is suppressed by an order of magnitude. Temperature-dependent SHG measurements in combination with Raman spectroscopy indicate a continuous order-disorder type polar phase transition at 140 K. Linear and nonlinear optical microscopy reveal 109°/71° ferroelastic domain walls, like in other trigonal ferroelectrics. No 180° polar domain walls are observed to emerge across the phase transition.

PACS numbers: Valid PACS appear here

Keywords: polar metal, nonlinear optics, second harmonic generation, ferroelectric domains

Polar metals are a relatively rare class of materials that exhibit ferroelectric-like long-range polar order in a metallic state¹⁻³. These materials are of much interest because of the seeming incompatibility of polar order and metallicity, since free electrons in a metal are typically expected to screen the long-range electrostatic forces that stabilize polar ordering. The recent identification¹ of a ferroelectric-like phase transition in metallic lithium osmate (LiOsO₃) has led to a flurry of activity²⁻⁷ to understand the origin of polar metallicity in these materials. From the point of view of applications, a ferroelectric-like structure in a metallic state leads to another intriguing question - how do functional properties typical of insulating ferroelectrics manifest themselves in a metal?

Optical properties are one such example, with the strong optical birefringence and nonlinear susceptibility of classical ferroelectrics such as LiNbO₃ and BaTiO₃ finding extensive application in optical materials and in optoelectronic devices⁸. Nonlinear optical processes are also the foundation behind several important condensed matter phenomena such as higher harmonic generation⁸, the optical Kerr effect, and photo-induced shift current⁹. In this context, it is of interest to study and understand the optical properties of this unique class of polar materials. A recent study has reported¹⁰ that polar metals in the family of TaAs exhibit a giant nonlinear optical coefficient, with an enhanced response along

the polar direction, providing further motivation for the present study. In this work, we consider one of the first identified¹ polar metals, LiOsO₃. It is notable that this material has a lattice structure and polar phase transition that are isostructural to the ubiquitous insulating optical nonlinear materials LiNbO₃ and LiTaO₃¹. A study of the optical properties of LiOsO₃ would hence be of interest not only from the point of view of potential applications, but also as a model system to understand the role of metallicity in the emergence of these properties. Furthermore, the nonlinear optical response can be used as a sensitive probe of important physical quantities such as spontaneous polarization¹¹, and phenomena such as phase transitions^{11,12}, ferroic domain formation⁸, and coupling between different order parameters¹¹, all of which are critical to understanding the physics underlying this unique class of materials. Characterization methods based on nonlinear optics assume further importance given that the presence of free carriers makes it difficult to study these materials using traditional techniques like piezo-force microscopy and P-E loop measurements.

In this work, the linear and nonlinear optical properties of single crystal LiOsO₃ were measured using spectroscopic ellipsometry and optical second harmonic generation (SHG) at a fundamental wavelength of 800 nm. Strong optical birefringence was observed in the complex linear refractive index. The optical SHG tensor coefficients extracted from SHG polarimetry revealed that the susceptibility along the polar direction is suppressed by an order of magnitude, compared to isostructural in-

^{a)} Electronic mail: vxg8@psu.edu

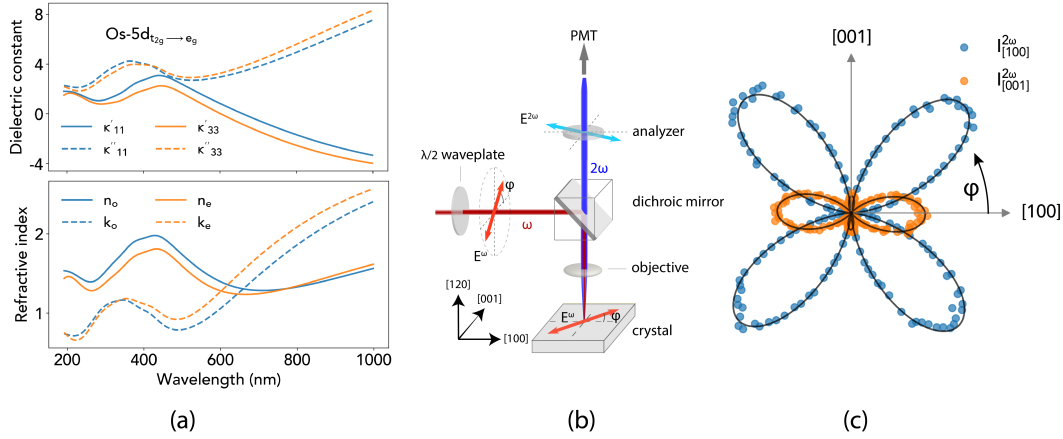


FIG. 1. (a) Linear optical constants at 300 K obtained from spectroscopic ellipsometry. The top panel shows the dielectric constant, $\kappa = \kappa' + i\kappa''$, and the lower panel shows the refractive index $\tilde{n} = n + ik$. The parameters of the Lorentz oscillators used to fit the ellipsometry data can be found in Fig. S2. Figure (b) shows a schematic of the optical setup used for SHG polarimetry, and (c) the measured SHG polar plots at 20 K. The black lines are theory fits to 3m point group symmetry.

insulating ferroelectrics LiNbO₃ and LiTaO₃, as a consequence of the weak coupling mechanism² that stabilizes the polar metal phase in LiOsO₃. We then use SHG in combination with Raman spectroscopy as a probe of the unique ferroelectric-like phase transition in LiOsO₃. These measurements showed that the polar phase transition in LiOsO₃ is continuous, exhibiting signatures of an order-disorder nature, with long-range order setting in at around 80 K. Linear and nonlinear optical microscopy and electron backscattering diffraction are used to identify 109°/71° ferroelastic domain walls. No 180° polar domain walls were observed across the phase transition.

Optical second harmonic generation (SHG) is a second order nonlinear optical response to incident electromagnetic radiation. In this process, light incident on a material at frequency ω is converted into light at frequency 2ω , through the creation of a nonlinear polarization in the material, $P_i^{2\omega} = \epsilon_0 \chi_{ijk}^{(2)} E_j^\omega E_k^\omega$, where $P^{2\omega}$ is the second harmonic polarization, \vec{E}^ω is the electric field of the incident light, and $\chi^{(2)}$ is the optical SHG susceptibility tensor. With $\chi^{(2)}$ being an odd ranked tensor, a non-zero SHG response is only allowed in noncentrosymmetric materials. SHG is thus a sensitive probe of inversion symmetry breaking, whether it is at interfaces such as surfaces, or in the bulk, through electric dipoles and multipoles. The bulk contribution is expected to dominate over the surface contribution⁸. It is noteworthy that results of common theoretical models used to describe SHG, based on the anharmonic Lorentz oscillator, such as Miller's rule¹³ and Kleinman symmetry^{13,14}, would in principle be invalid in polar metals, due to the finite intraband absorption associated with the lack of a bandgap.

LiOsO₃ single crystals were grown using solid state reaction under high pressure, as in the previous work by Shi et al¹. First, spectroscopic ellipsometry was used to obtain the linear optical constants at 300 K, between 200 nm and 1000 nm. The ellipsometry data was fitted using Lorentz oscillators (see Fig. S2), and the complex dielectric function $\tilde{\kappa}$ and refractive index \tilde{n} were extracted. The complex dielectric function plotted in Fig. 1a shows

a strong absorption at around 350 nm, which likely corresponds to Os-5d interband transitions from occupied t_{2g} states to e_g states above the Fermi energy¹⁵. Notably, significant anisotropy is observed between the hexagonal [100] and [001] directions, contrary to previously reported data⁷. This anisotropy is likely primarily due to the Os-5d interband absorption, which was not accounted for in the reported work. The complex refractive indices in Fig. 1a are used in the subsequent analysis of the measured nonlinear optical constants.

The SHG tensor coefficients of LiOsO₃ were probed using SHG polarimetry as follows. The measurements were done in a far-field reflection geometry at normal incidence. The fundamental was a pulsed laser beam from a Ti:sapphire femtosecond laser with a wavelength of 800 nm (pulse width 80 fs, repetition rate 80 MHz). A beam with a power of 20 mW was focused on the (120) surface of a LiOsO₃ single crystal using a 50x objective, onto a spot size of $\sim 0.5 \mu\text{m}$. SHG polarimetry was done following the schematic in Fig. 1b. The crystal was aligned so that the [120] axis was coincident with the fundamental, while the [100] and [001] were along mutually perpendicular directions in the plane of the probed surface. It was confirmed using electron back-scattering diffraction that the probed region was a single domain. The fundamental was linearly polarized, with the polarization within the (120) plane, making an angle ϕ with [100]. The reflected second harmonic light was collected using a photomultiplier tube, after passing through an analyzer. Note that all Miller indices are in the hexagonal setting.

Since LiOsO₃ is centrosymmetric (space group $R\bar{3}c$) at room temperature, the SHG at room temperature is likely primarily from inversion symmetry breaking at the surface and multipole contribution of bulk charges. The detector was calibrated so as to set this as the zero level. Measurements were then carried out at 20 K, which is below the reported¹ non-polar ($R\bar{3}c$) to polar ($R3c$) phase transition temperature of 140 K. A pair of complementary polar plots were obtained by measuring the SHG signal as a function of the polarization of the fundamen-

tal, ϕ , with the analyzer oriented along the [100] direction ($I_{[100]}^{2\omega}(\phi)$), and [001] direction ($I_{[001]}^{2\omega}(\phi)$), shown in Fig. 1c. To obtain the SHG tensor coefficients, these experimental polar plots were fitted to a theoretical model based on the $3m$ point group symmetry of LiOsO₃. The third rank tensor χ_{ijk} is usually written using the Voigt notation d_{ij} , in a pseudomatrix form. For $3m$ symmetry, the non-zero coefficients of d_{ij} are $d_{15} = d_{24}$, $-d_{22} = d_{16} = d_{21}$, $d_{31} = d_{32}$, and d_{33} . Note that since LiOsO₃ is a metal with finite dispersion in the spectral range of interest, Kleinman symmetry, which allows for the permutation of certain tensor indices for materials that are dispersionless, is violated. The associated additional condition $d_{15} = d_{31}$ that is valid for isostructural insulators LiNbO₃ and LiTaO₃ is thus invalid for LiOsO₃.

Since the fundamental was linearly polarized in the (120) plane, $E_1 = E_0 \cos(\phi)$, $E_2 = 0$, and $E_3 = E_0 \sin(\phi)$. With the analyzer oriented along the [100] and [001] directions, the theoretical expressions for the two polar plots respectively simplify to

$$\begin{aligned} I_{[100]}^{2\omega}(\phi) &= |E_{[100]}^{2\omega}(\phi)|^2 \propto |d_{15} E_0^2 \sin^2(2\phi)|^2 \\ I_{[001]}^{2\omega}(\phi) &= |E_{[001]}^{2\omega}(\phi)|^2 \propto |d_{31} E_0^2 \cos^2(\phi) + d_{33} E_0^2 \sin^2(\phi)|^2. \end{aligned} \quad (1)$$

As Eq. 1 shows, d_{22} is not accessible using the (120) surface at normal incidence. This was instead obtained through an additional measurement at an angle of incidence of 45° (see Fig. S3). The experimental polar plots were fitted to these equations to obtain the ratios of the d_{ij} coefficients. The SHG signal was calibrated with respect to congruently grown (001) LiTaO₃ to estimate the absolute magnitude of the coefficients. The expression derived by Bloembergen and Pershan¹⁶ was used to account for changes in reflectance due to differences in the linear refractive indices of LiTaO₃¹⁷ and LiOsO₃. The results are tabulated in Table 1, and the values of the SHG tensor coefficients of LiNbO₃ and LiTaO₃ are also given for comparison.

Although d_{15} , d_{22} , and d_{31} are of the same order of magnitude across all three materials, d_{33} is lower by an order of magnitude in LiOsO₃. This behavior appears to be a consequence of the different coordination environment of Li and transition metal ($M = \text{Nb, Ta, Os}$) cations within the octahedra comprising the structures. In general the anharmonicity and associated optical nonlinearity in this family of materials are more sensitive to M-O acentric displacements than Li-O acentric displacements because of the larger nominal ionic charge on M ions compared to Li ions. LiOsO₃ exhibits substantially smaller M-O acentric displacements due to the weak coupling mechanism² that stabilizes the polar metal state. This can be seen in the length of the long (l) and short (s) M-O bonds of LiOsO₃, as compared to those in LiNbO₃ and LiTaO₃, listed in Table S2. Qualitatively, the ratio of these bond lengths projected onto the [001] and [100] directions can be related to the degree of anharmonicity along these two directions, and hence to the SHG coefficients associated with them¹⁸⁻²⁰. That is, M-O(l)/M-O(s) projected along [001] will affect d_{33} , whereas M-O(l)/M-O(s) projected along [100] will affect d_{22} and d_{31} .

TABLE I. SHG tensor coefficients of LiOsO₃ in pm/V, obtained from polar plots at 20 K, with those of LiNbO₃ and LiTaO₃ for comparison. Error bars are shown in parentheses.

d_{ij}	LiOsO ₃ ^a	LiNbO ₃ ^b	LiTaO ₃ ^b
d_{15}	± 2.8 (0.4)	-5.2 (0.8)	-1.1 (0.2)
d_{31}	∓ 1.9 (0.2)	-5.2 (0.8)	-1.1 (0.2)
d_{22}	∓ 2.3 (0.3)	2.8 (0.2)	1.9 (0.2)
d_{33}	± 0.93 (0.1)	-36.3 (8.9)	-17.5 (2.2)

^a Values at 800 nm, 20 K from present work.

^b Values at 1060 nm, 300 K from reference 21.

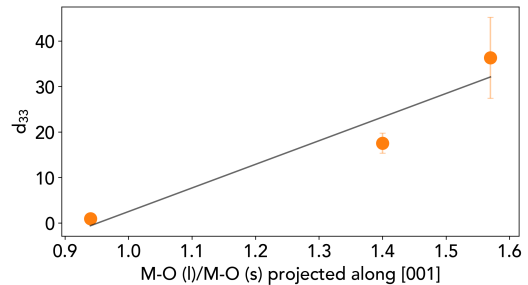


FIG. 2. The variation in d_{33} as a function of MO₆ acentric displacements along [001], as quantified by the ratio of the [001] projections of long (l) and short (s) M-O bonds in LiMO₃ with $M = (\text{Nb, Ta, Os})$. Bond lengths are taken from references 22, 23, and 1 respectively, and d_{33} values from 21.

Fig. 2 shows that the [001] projection of the acentric M-O displacements decreases significantly going from LiNbO₃ to LiOsO₃, which explains the suppressed d_{33} in LiOsO₃. On the other hand, the [100] projection is relatively uniform (see Table S3), due to which d_{22} and d_{31} are each of the same order of magnitude across all three materials. A more in-depth analysis of this behavior is of interest, and will be the subject of future work.

The SHG response was also probed as a function of temperature to characterize the polar phase transition. The temperature detector was calibrated using a reference sample with a known phase transition. The absolute SHG signal as a function of temperature is plotted in Fig. 3, while the temperature dependence of the coefficients can be found in Fig. S4. The SHG response indicates a continuous polar phase transition with an onset near 135 K. The exact phase transition temperature is difficult to pinpoint because the signal is very close to the noise floor near the phase transition (see inset of Fig. 3). The fact that the signal is negligible above the phase transition temperature, and drastically increases as the temperature decreases below it indicates that the SHG response as probed in this geometry is strongly coupled to the dipoles in the bulk, and that this coupling dominates over other contributions. In fact the SHG response is coupled to the polar order parameter by a free energy term in the centrosymmetric phase (point group symmetry $\bar{3}m$) given by $F = -\chi_{ijkl} E_i^{2\omega} E_j^\omega E_k^\omega Q_l$, where E^ω refers to the fundamental electric field, $E^{2\omega}$ refers to the second harmonic electric field, and Q refers to the order parameter corresponding to polar displacements. It can be shown^{11,24} that this term, which is zero above the phase transition

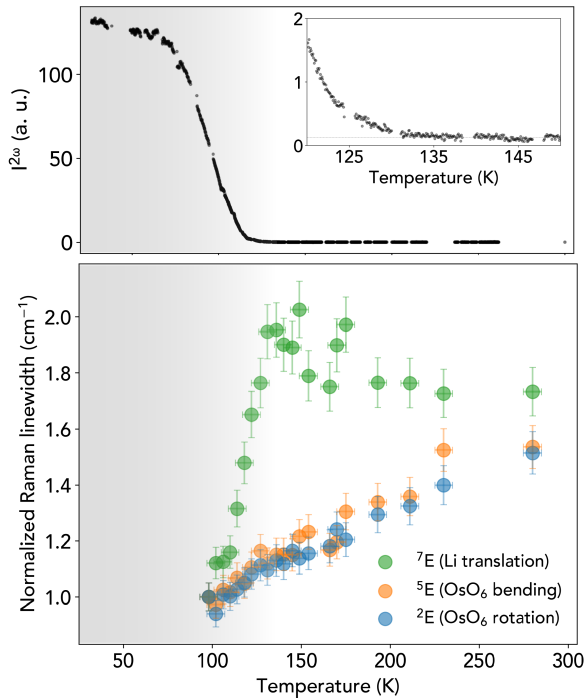


FIG. 3. The temperature dependence of SHG is shown in the upper panel, with an enlarged plot of the dependence near the phase transition shown in the inset. The lower panel shows the Raman linewidths of three different phonon modes as a function of temperature, with 2E , 5E , and 7E corresponding to modes at frequencies of 206 cm^{-1} , 402 cm^{-1} , and 492 cm^{-1} respectively, at room temperature.

temperature T_0 , evolves into $F = -[\chi_{ijk3}Q_3]E_i^{2\omega}E_j^\omega E_k^\omega$, which is nothing but $-P_i^{2\omega}E_i^{2\omega}$, the energy due to interaction between second harmonic electric field and polarization induced by a second order nonlinear optical susceptibility $\chi_{ijk}(T < T_0) = \chi_{ijk3}Q_3$. The SHG susceptibility χ_{ijk} is thus linearly proportional to the polar order parameter Q , and the measured SHG response $I^{2\omega}$ is proportional to Q^2 . The temperature dependence of the SHG response in the present study is thus an indirect probe of the polar order parameter across the phase transition in LiOsO₃.

The SHG response and the associated polar order parameter gradually increase as the sample is cooled below 140 K, before increasing rapidly and saturating at around 80 K, as seen in Fig. 3a. It is pertinent to ask whether this behavior is due to the occurrence of an order-disorder phase transition as opposed to a displacive phase transition, as this is a point of contention in the literature^{1,6,15,25}. To shed more light on this, Raman spectroscopy measurements were carried out to study the behavior of phonon modes across the phase transition. Temperature increase due to laser heating was taken into account using the Stokes-anti-Stokes relationship. To begin with, no Raman active soft modes that might result in a displacive phase transition were observed in the Raman spectra, consistent with previous studies²⁵. Raman linewidths are directly related to disorder in the system, and hence when studied as a function of temperature, can be used to identify order-disorder

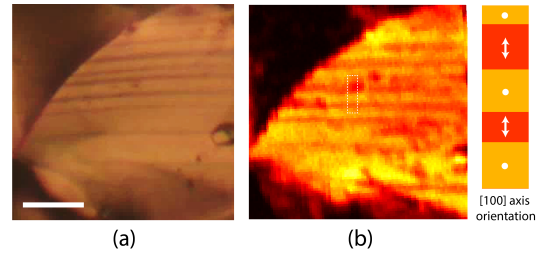


FIG. 4. Ferroelastic domains in LiOsO₃ with (a) showing a linear optical micrograph at 300 K, and (b) a nonlinear optical micrograph using SHG reflectance at 20 K. A schematic of the domains is shown on the right, with the arrows denoting the direction of the [100] crystallographic axis, obtained from electron back-scattering diffraction (see Fig. S5). The scale bar in (a) is 10 μm .

phase transitions, as done in previous work on complex oxides^{26,27}. Previous studies showed a large decrease in Raman peak linewidths below 140 K, and attributed that to the order-disorder nature of the phase transition²⁵. In the present work, we repeat these measurements and expand on the analysis, paying particular attention to the Raman modes corresponding to displacements of Li atoms. The proposed order-disorder transition consists of ordering of off-centered Li atoms, so it is reasonable to expect that if the phase transition is indeed order-disorder in nature, the Raman phonon modes consisting of Li displacements would exhibit the largest change in linewidth. The linewidths of the three dominant E modes (see Fig. S5 for peak labels) are plotted in Fig. 3b, of which only one, 7E , involves the displacement of Li atoms. Clearly this mode, consisting of antiparallel Li translation perpendicular to the polar direction, shows the largest increase in linewidth, with a clear discontinuity in the slope near the critical temperature. This linewidth increase is more than twice that of the 2E and 5E modes, which consist of OsO₆ octahedra bending and rotation respectively. Additionally, the present measurements were limited to around 98 K, but the Raman peak linewidths in the work by Jin et al²⁵, with data collected down to 10 K, appear to saturate at the same temperature as the SHG response in the present work, at around 80 K, providing further evidence that these two results may be complementary signatures of the onset of long-range polar order through an order-disorder transition.

Finally, linear and nonlinear optical microscopy was used to study the influence of the ferroelectric-like phase transition on the mesoscale structure of LiOsO₃. The linear optical micrograph in Fig. 4a shows a striped domain structure observed in the nonpolar phase. These stripes were oriented using electron back-scattering diffraction (EBSD) (see Fig. S6) and identified as ferroelastic domains, with the [100] crystallographic axes in adjacent domains forming an angle of 90° relative to each other, as shown in Fig. 4b. This geometry is consistent with 71°/109° polar domain walls formed by the breaking of four-fold symmetry in the lattice, going from a high temperature cubic $Pm\bar{3}m$ structure to the room temperature trigonal $R\bar{3}c$ structure. The sample surface was also studied using scanning SHG microscopy at 20 K.

The SHG map confirms that these domains are polar below the phase transition, and the contrast between stripes is consistent with the EBSD orientation information. Such measurements can also be used to identify any additional 180° ferroelectric domains that nucleate across the nonpolar-to-polar phase transition in the form of suppressed SHG intensity at domain walls^{8,28}. However, there were no such domains observed, despite the presence of ferroelastic domain walls, which are generally expected to be preferential nucleation sites for such features. This observation, while surprising for a polar material, is consistent with the metallic nature of LiOsO₃. In insulating ferroelectrics, the depolarizing field created by ordered electric dipoles destabilizes a single domain configuration and drives the formation of 180° polar domains^{29,30}. Such a depolarizing field would be expected to be screened by free electrons in a metal such as LiOsO₃, allowing the single domain configuration to be stable.

To summarize, the linear and nonlinear optical properties of LiOsO₃ were measured, and used to probe its unique polar phase transition. The optical SHG susceptibility was found to be suppressed along [001] owing to a reduction in the Os-O bond anisotropy along the polar axis. Temperature-dependent SHG and Raman measurements were consistent with the occurrence of a continuous order-disorder phase transition at 140 K. Polar ferroelastic domains were observed using SHG microscopy, however no 180° domain walls were observed.

SUPPLEMENTARY MATERIAL

The supplementary material contains detailed information on the crystal orientation using electron back-scattering diffraction, spectroscopic ellipsometry, SHG polarimetry, supporting information for the bond anisotropy, and complete Raman spectra over the measured temperature range.

ACKNOWLEDGEMENTS

H.P., Y.Y., V.G., Y.C., and J.C. acknowledge DOE grant de-sc0012375 for SHG microscopy, sample preparation, and bond anisotropy analysis. H.P., Y.P., and V.G. acknowledge NSF MRSEC CNS grant DMR-1420620 for ellipsometry and Raman studies. D.P. and J.M.R. were supported by ARO (W911NF-15-1-0017). J.C. was supported by the Gordon and Betty Moore Foundation EPiQS Initiative through grant GBMF4534. Y.S. acknowledges National Natural Science Foundation of China grants 11774399, 11474330, and the Chinese Academy of Sciences grants XDB07020100 and QYZDB-SSW-SLH043, and also Kazunari Yamaura in National Institute for Materials Science (NIMS) of Japan for providing high quality LiOsO₃ single crystals. L.G. acknowledges NSF grants DMR-0805073, DMR-0958349, DMR-1429428, Office of Naval Research Award No. N00014-06-1-013, and UNF Terry Presidential Professorship.

H.P. and V.G. acknowledge useful discussions with David Hsieh. H.P. acknowledges Maxwell Wetherington and Julie Anderson for help with sample characterization.

REFERENCES

- Y. Shi, Y. Guo, X. Wang, A. J. Princep, D. Khalyavin, P. Manuel, Y. Michiue, A. Sato, K. Tsuda, S. Yu, M. Arai, Y. Shirako, M. Akaogi, N. Wang, K. Yamaura, and A. T. Boothroyd, *Nature Materials* **12**, 1024 (2013).
- D. Puggioni and J. M. Rondinelli, *Nature Communications* **5**, 3432 (2014), arXiv:arXiv:1310.1148v1.
- N. A. Benedek and T. Birol, *Materials Chemistry C* **4**, 4000 (2016), arXiv:1511.06187.
- H. J. Xiang, *Physical Review B* **90**, 094108 (2014).
- G. Giovannetti and M. Capone, *Physical Review B* **90**, 3 (2014).
- H. Sim and B. G. Kim, *Physical Review B* **89**, 1 (2014).
- I. Lo Vecchio, G. Giovannetti, M. Autore, P. Di Pietro, A. Perucchi, J. He, K. Yamaura, M. Capone, and S. Lupi, *Physical Review B* **93**, 161113 (2016).
- S. A. Denev, T. T. A. Lummen, E. Barnes, A. Kumar, and V. Gopalan, *Journal of the American Ceramic Society* **94**, 2699 (2011).
- T. Morimoto and N. Nagaosa, *Science advances* **2**, e1501524 (2016), arXiv:1510.08112.
- L. Wu, S. Patankar, T. Morimoto, N. L. Nair, E. Thewalt, A. Little, J. G. Analytis, J. E. Moore, and J. Orenstein, *Nature Physics* **13**, 350 (2017), arXiv:1609.04894.
- M. O. Ramirez, A. Kumar, S. A. Denev, N. J. Podraza, X. S. Xu, R. C. Rai, Y. H. Chu, J. Seidel, L. W. Martin, S. Y. Yang, E. Saiz, J. F. Ihlefeld, S. Lee, J. Klug, S. W. Cheong, M. J. Bedzyk, O. Auciello, D. G. Schlom, R. Ramesh, J. Orenstein, J. L. Musfeldt, and V. Gopalan, *Physical Review B* **79**, 1 (2009).
- J. W. Harter, Z. Y. Zhao, J.-Q. Yan, D. G. Mandrus, and D. Hsieh, *Science* **356**, 295 (2017).
- R. W. Boyd, *Nonlinear optics* (Academic press, 2003).
- C. A. Dailey, B. J. Burke, and G. J. Simpson, *Chemical Physics Letters* **390**, 8 (2004).
- H. M. Liu, Y. P. Du, Y. L. Xie, J. M. Liu, C. G. Duan, and X. Wan, *Physical Review B* **91**, 2 (2015), arXiv:1409.4953.
- P. S. Bloembergen, N. and Pershan, *Physical Review* **128** (1962).
- A. Bruner, D. Eger, M. B. Oron, P. Blau, M. Katz, and S. Ruschin, , 66 (2002).
- T. T. Tran, P. S. Halasyamani, and J. M. Rondinelli, *Inorganic Chemistry* **53**, 6241 (2014).
- A. Cammarata and J. M. Rondinelli, *ACS Photonics* **1**, 96 (2014).
- A. Cammarata, W. Zhang, P. S. Halasyamani, and J. M. Rondinelli, *Chemistry of Materials* **26**, 5773 (2014).
- R. C. Miller and A. Savage, *Applied Physics Letters* **9**, 169 (1966).
- S. Abrahams, J. M. Reddy, and J. Bernstein, *Journal of Physics and Chemistry of Solids* **27**, 997 (1966).
- S. Abrahams and J. Bernstein, *Journal of Physics and Chemistry of Solids* **28**, 1685 (1967).
- D. Sa, R. Valentí, and C. Gros, *The European Physical Journal B* **14**, 301 (2000), arXiv:0803.2201.
- F. Jin, A. Zhang, J. Ji, K. Liu, L. Wang, Y. Shi, Y. Tian, X. Ma, and Q. Zhang, *Physical Review B* **93**, 1 (2016).
- M. K. Singh, N. K. Karan, R. S. Katiyar, J. F. Scott, and H. M. Jang, *Journal of Physics Condensed Matter* **20** (2008), 10.1088/0953-8984/20/5/055210.
- M. K. Singh, G. Singh, T. H. Kim, S. Kojima, R. S. Katiyar, and J. F. Scott, *EPL (Europhysics Letters)* **107**, 26004 (2014).
- S. Lei, M. Gu, D. Puggioni, G. Stone, J. Peng, J. Ge, Y. Wang, B. Wang, Y. Yuan, K. Wang, Z. Mao, J. M. Rondinelli, and V. Gopalan, *Nano Letters* **0**, null (0), pMID: 29631404.
- M. E. Lines and A. M. Glass, *Principles and applications of ferroelectrics and related materials* (Oxford university press, 1977).
- J. Guyonnet, in *Ferroelectric Domain Walls* (Springer, 2014) pp. 7-24.